Check for updates

ADVANCING EARTH AND SPACE SCIENCES

Geophysical Research Letters

RESEARCH LETTER
10.1029/2024GL111745

A Case Study on the Impact of Interplanetary Coronal Mass Ejection on the Martian O(^{1}S) 557.7 nm Dayglow Emission Using ExoMars TGO/NOMAD-UVIS Observations: First Results

Aadarsh Raj Sharma[1], **Lot Ram**[1], **Harshaa Suhaag**[1], **Dipjyoti Patgiri**[1], **Lauriane Soret**[2], **Jean-Claude Gérard**[2], **Ian R. Thomas**[3], **Ann Carine Vandaele**[3], **and Sumanta Sarkhel**[1,4]

[1]Department of Physics, Indian Institute of Technology Roorkee, Roorkee, India, [2]LPAP, STAR Institute, University of Liège, Liège, Belgium, [3]Royal Belgian Institute for Space Aeronomy, Brussels, Belgium, [4]Centre for Space Science and Technology, Indian Institute of Technology Roorkee, Roorkee, India

Key Points:

- Impact of interplanetary coronal mass ejections (ICME) on the Martian 557.7 nm dayglow emission has been studied using instruments onboard ExoMars-TGO and Mars Atmosphere and Volatile Evolution spacecrafts
- During ICMEs, the primary emission peak does not show variation compared to quiet-time and seasonal quiet-time average periods
- An enhancement in the secondary emission peak and upper altitude region (140–180 km) is observed due to increased electron impact process

Supporting Information:

Supporting Information may be found in the online version of this article.

Correspondence to:

S. Sarkhel,
sarkhel@ph.iitr.ac.in

Citation:

Sharma, A. R., Ram, L., Suhaag, H., Patgiri, D., Soret, L., Gérard, J.-C., et al. (2025). A Case study on the impact of interplanetary coronal mass ejection on the Martian O(^{1}S) 557.7 nm dayglow emission using ExoMars TGO/NOMAD-UVIS observations: First results. *Geophysical Research Letters*, *52*, e2024GL111745. https://doi.org/10.1029/2024GL111745

Received 2 AUG 2024
Accepted 19 FEB 2025

Author Contributions:

Conceptualization: Sumanta Sarkhel
Formal analysis: Aadarsh Raj Sharma, Lot Ram, Harshaa Suhaag
Investigation: Sumanta Sarkhel
Methodology: Aadarsh Raj Sharma, Sumanta Sarkhel
Supervision: Sumanta Sarkhel
Writing – original draft: Aadarsh Raj Sharma, Lot Ram, Harshaa Suhaag, Dipjyoti Patgiri, Lauriane Soret, Jean-Claude Gérard, Ian R. Thomas, Ann Carine Vandaele, Sumanta Sarkhel

Abstract

We report, for the first time, the impact of interplanetary coronal mass ejections (ICME) on the recently discovered O(^{1}S) 557.7 nm dayglow emission in the Martian atmosphere. While there are a few studies on the seasonal variation of 557.7 nm dayglow emission available in the literature, the impact of ICME has not been investigated so far. Using the instruments aboard the ExoMars-TGO and Mars Atmosphere and Volatile Evolution (MAVEN) spacecraft, we show that the primary emission peak (75–80 km) remains unaffected during ICME events compared to quiet-times. However, an enhancement has been observed in the brightness of the secondary emission peak (110–120 km) and the upper altitude region (140–180 km). The enhancement is attributed to the increased solar electrons, X-ray fluxes and Solar Energetic Particles, augmenting the electron-impact processes causing the enhancement in the brightness. Thus, this study has an implication to the brightness of Martian upper atmosphere during intense solar transients like ICME.

Plain Language Summary

The O(^{1}S) 557.7 nm dayglow emission has been recently discovered in the Martian dayside atmosphere, having a primary and secondary emission peak observed at ∼80 and ∼120 km altitudes, respectively. It is produced via photodissociation of CO_2 by solar extreme ultraviolet radiation and electron impact processes. It is to be noted that space weather events like interplanetary coronal mass ejection (ICME) can significantly affect the Martian atmosphere. This motivates us to study the behavior of 557.7 nm emission during ICME events. This study reports, for the first time, the impact of ICME on the O(^{1}S) 557.7 nm dayglow emission using the instruments onboard ExoMars-TGO and MAVEN spacecrafts. Our findings show that during the ICME, the primary emission peak does not show any variation as compared to quiet-times. However, the brightness of secondary emission peak and upper-altitude region (140–180 km) show enhancements in comparison to quiet-times. We have observed an increase in the solar X-ray, electron fluxes and Solar Energetic Particles during the ICME events which produces more photoelectrons and secondary electrons. This enhances the electron impact process resulting in the enhancement in the brightness of the secondary emission peak and the upper altitude region.

1. Introduction

The detection of O(^{1}S) 557.7 nm Martian dayglow emission was recently reported by Gérard et al. (2020) using the Ultraviolet and Visible Spectrometer (UVIS) channel part of Nadir and Occultation for Mars Discovery (NOMAD) onboard Exobiology on Mars–Tracer Gas Orbiter (ExoMars-TGO) mission of European Space Agency (ESA) and ROSCOSMOS. They found that the 557.7 nm limb profiles consist of two peaks with a primary emission peak altitude near 80 km and a secondary peak near 120 km. Various photochemical reactions are responsible for producing O(^{1}S) state, which involves plasma and solar radiation (Gkouvelis et al., 2018; Jain, 2013; Raghuram et al., 2021). The primary reactions, involving photodissociation and photoelectron impact on CO_2, CO and O_2 and dissociative recombination of CO_2^+ and O_2^+, are as follows:

$$CO_2 + h\nu \rightarrow O(^1S) + CO \quad \text{(R1)}$$

Geophysical Research Letters 10.1029/2024GL111745

Writing – review & editing: Aadarsh Raj Sharma, Lot Ram, Harshaa Suhaag, Dipjyoti Patgiri, Lauriane Soret, Jean-Claude Gérard, Ian R. Thomas, Ann Carine Vandaele, Sumanta Sarkhel

$$CO + h\nu \rightarrow O(^1S) + C \quad (R2)$$

$$O_2 + h\nu \rightarrow O(^1S) + O \quad (R3)$$

$$O + e^* \rightarrow O(^1S) + e^* \quad (R4)$$

$$CO_2 + e^* \rightarrow O(^1S) + CO + e^* \quad (R5)$$

$$CO + e^* \rightarrow O(^1S) + C + e^* \quad (R6)$$

$$O_2 + e^* \rightarrow O(^1S) + O + e^* \quad (R7)$$

$$O_2^+ + e^- \rightarrow O(^1S) + O \quad (R8)$$

$$CO_2^+ + e^- \rightarrow O(^1S) + CO \quad (R9)$$

The variation of 557.7 nm dayglow emission between 60 and 200 km altitude, covers both the lower and upper atmosphere of Mars. The upper atmosphere, dominated by photo-ionization and photo-excitation, forms the ionosphere with M2 and M1 layers (Bougher et al., 2017; Rishbeth & Mendillo, 2004; Withers, 2020; Withers et al., 2018). The M2 layer (120–160 km) is produced by extreme ultraviolet (EUV) photons and contains the peak electron density, while the M1 layer (105–115 km) is formed by shorter wavelength X-ray photons (<15 nm) (Rishbeth & Mendillo, 2004; Withers, 2020; Withers et al., 2018). High energy X-rays generate hot photo-electrons, ionizing neutral species and creating ion-electron pairs (Fallows et al., 2015; Fox, 2004; Fox & Yeager, 2006). Photo-ionization and photoelectron ionization produce ${CO_2}^+$ as major ionic species, but it quickly gets removed through various reactions, leading to ${O_2}^+$, making it the primary ion at overall altitudes (Fox & Dalgarno, 1979). During passage of ICMEs, depletion has been observed in the Martian dayside and nightside plasma density (Jakosky, Grebowsky, et al., 2015; Ram et al., 2023; Thampi et al., 2021). Further, the peak electron density (M2 peak) of the ionosphere shows depletion with the upliftment of the peak (Ram, Rout, et al., 2024). The flares and ICMEs increase irradiance and electron flux that enhance ionization at 100–160 km, affecting Martian atmospheric emissions. For instance, flares can boost electron density by 50%–200% (Mendillo et al., 2006) and UV emissions by 50%–123% (Ram, Sharma, et al., 2024).

Recently, Soret et al. (2022) showed that the variation of 557.7 nm dayglow emission peaks over different seasons of Mars are in good agreement with photochemical airglow simulations. Although the long-term variations of the 557.7 nm dayglow have been studied, however, its behavior during transient events like ICME have not been investigated. This study, for the first time, takes advantage of simultaneous measurements of different instruments onboard ExoMars-TGO and Mars Atmosphere and Volatile Evolution (MAVEN) spacecraft to identify the ICMEs and observe their impact on the 557.7 nm dayglow emission.

2. Data and Methodology

The data used in this study has been collected from instruments onboard the ExoMars–TGO and MAVEN spacecraft. ExoMars-TGO orbits in a near-circular Martian orbit at ~400 km inclined by 74° on the planetary equator since 2018. Observations of $O(^1S)$ 557.7 nm were obtained using the UVIS (Patel et al., 2017; Vandaele et al., 2015) channel of NOMAD (Vandaele et al., 2018) instrument. We used special limb mode (inertial) data where the UVIS channel (usually pointing to the nadir) is oriented toward the planetary limb (López-Valverde et al., 2018). The UVIS spectrometer scans the Martian atmosphere in inertial limb mode from several hundreds of kilometers of altitude to the near-surface and back up toward the upper atmosphere, providing two scans (ingress and egress) in one orbit. The MAVEN satellite (Jakosky, Lin, et al., 2015) has been orbiting Mars since 2014 in 4.5 hr (currently ~3.5 hr) elliptical orbit with an apoapsis of ~6,200 km and periapsis altitude of ~150 km (currently ~180 km) and inclination of 75°. The solar wind parameters (velocity, density, and dynamic pressure), resultant interplanetary magnetic field (IMF; |**B**|) and electron density near Mars are obtained from Solar Wind Ion Analyzer (SWIA), Magnetometer (MAG), and Solar Wind Electron Analyzer (SWEA) instruments onboard the MAVEN spacecraft. The Extreme Ultraviolet Monitor (EUVM; Eparvier et al., 2015) part of the Langmuir

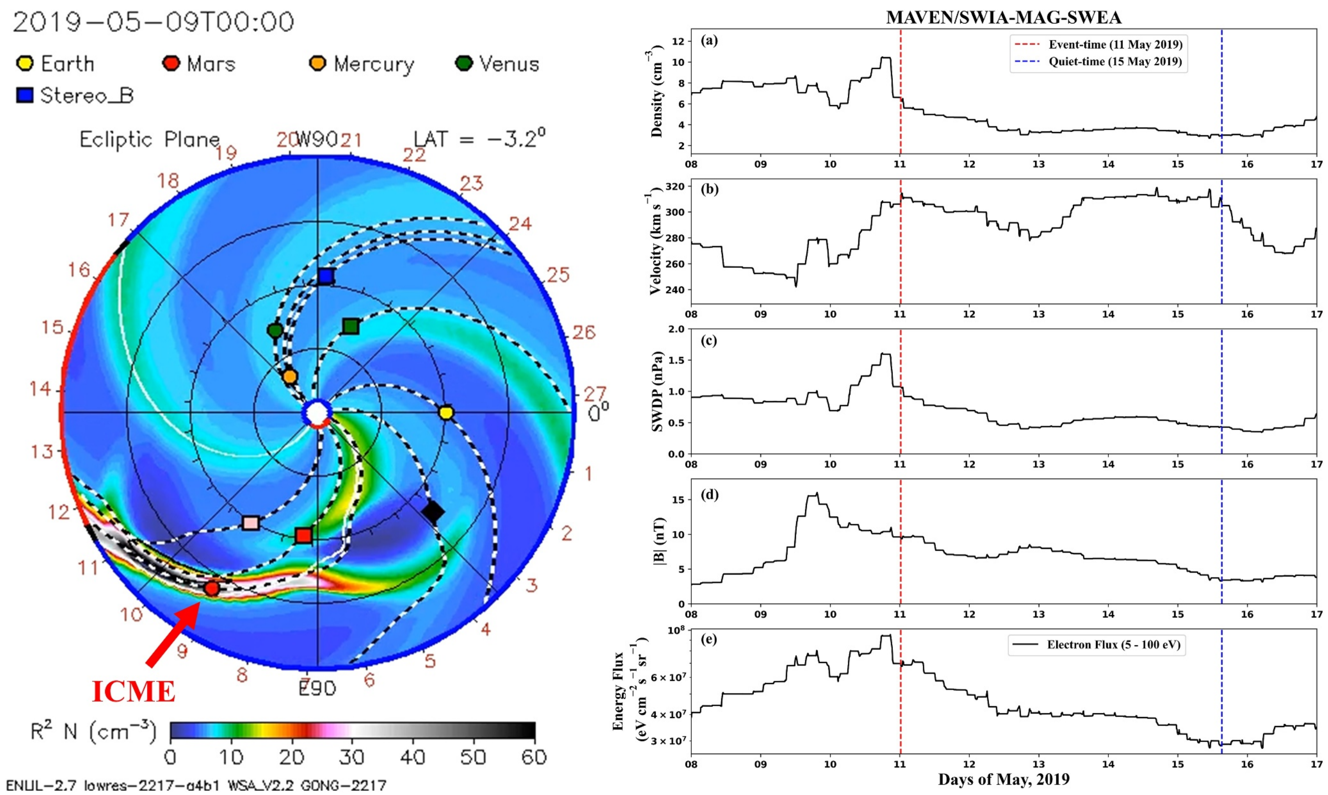

Figure 1. (Left) ENLIL-CONE model interplanetary coronal mass ejections simulation. (Right) Solar wind variations near Mars (08–17 May 2019): (a) density, (b) velocity, (c) dynamic pressure, (d) IMF (|**B**|), and (e) electron energy flux. Red and blue dashed lines indicate event and quiet-time NOMAD-UVIS observations.

Probe and Wave (LPW; Andersson et al., 2015) onboard MAVEN monitors the flux of solar irradiance. It measures the solar irradiance in three wavelength bands (0.1–0.7 nm, 17–22 nm, and 121.6 nm). SWIA measures the solar wind ion-flow and covers an energy range of 5 eV–25 keV (Halekas et al., 2015). The IMF is measured by the MAG using a triaxial fluxgate magnetometer (Connerney et al., 2015a, 2015b). SWEA is a symmetric, hemispheric electrostatic analyzer that measures the energy and angular distributions of 3–4,600 eV electrons (Mitchell et al., 2016). Solar Energetic Particle (SEP; Larson et al., 2015) instruments measure highly energetic SEP ions (energy 30–1,000 keV), and electrons (30–300 keV).

For this study, ICME events are identified through the Space Weather Database of Notifications (2010) archive. Those NOMAD-UVIS observations are considered which coincided with the ICME events. The UVIS dayside limb observations consist of spectral data for each tangent altitude, selected based on altitude, latitude, solar zenith angle (SZA), and Martian solar longitude (L_S). According to Gérard et al. (2020), the 557.7 nm emission is primarily observed between altitudes of 70–200 km in the dayside atmosphere of Mars. Consequently, all spectra are obtained between altitudes of 60–200 km with an SZA less than 70°. Spectral data below 100 km, affected by solar contamination, have been corrected using the methodology outlined by Aoki et al. (2022). First, the signal of $O(^1S)$ emission at 557.7 nm is considered between the spectral range of 556.2 and 559.2 nm at a given altitude. Subsequently, the average radiance values are also estimated in the wavelength range of (550.2–556.2 nm) and (559.2–565.2 nm) at that altitude. The background noise is then determined by taking the mean of the two average radiance values and then subtracted from the respective emission spectra to remove the solar contamination. In the subsequent step, the Radiance unit is converted from $W\text{m}^{-2}\ \text{nm}^{-1}\text{sr}^{-1}$ to kR nm^{-1} [kilo-Rayleigh (kR); 1 Rayleigh = 10^6 photons $\text{cm}^{-2}\ \text{s}^{-1}$ emitted in 4π steradians]. This procedure has been applied to UVIS limb observations gathered between April 2019 and October 2023.

3. Results

The limb profiles of 557.7 nm dayglow during the ICME event are compared with the quiet-time to assess the impact of the ICME. For verifying the upstream conditions, we have analyzed the data from SWIA,

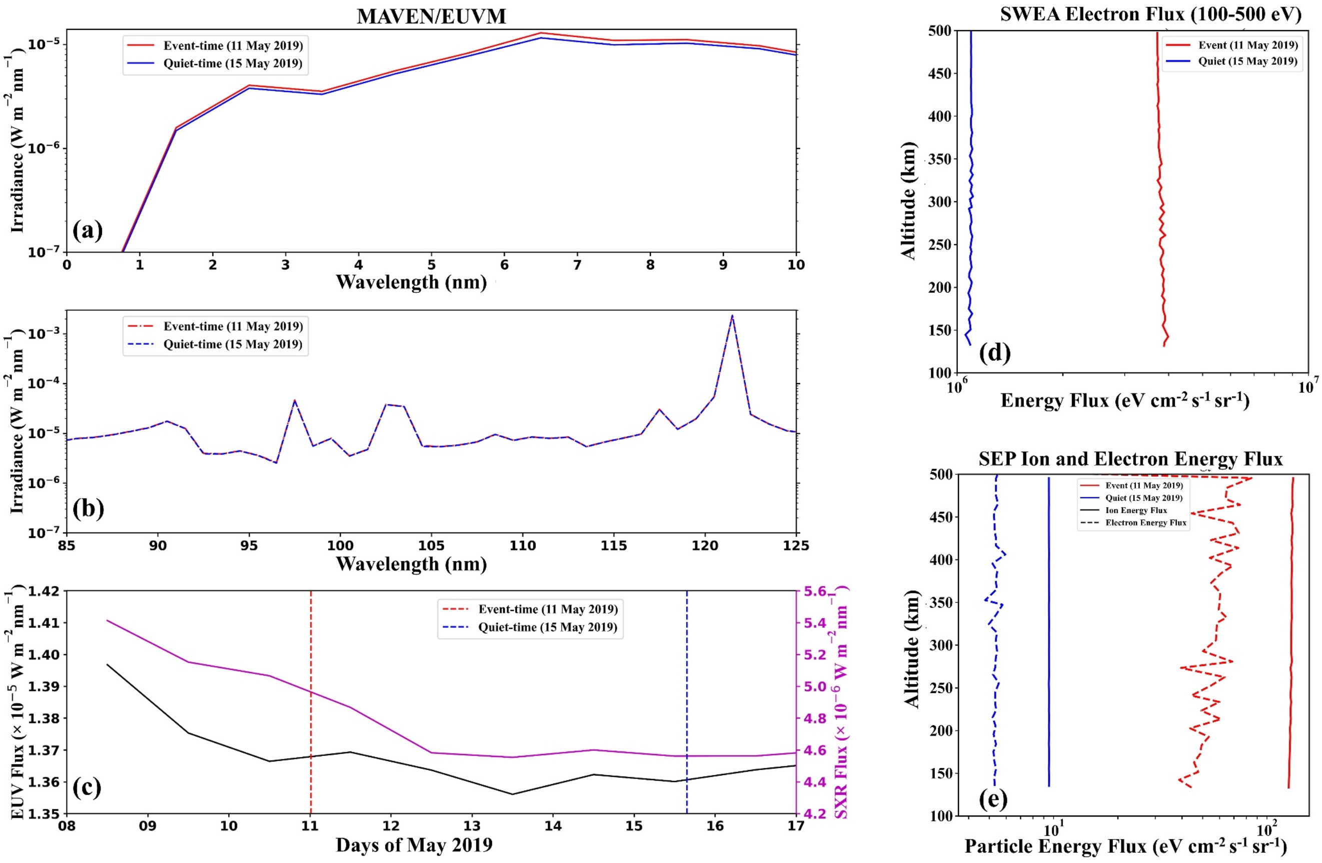

Figure 2. (a) SXR (1–10 nm) and (b) EUV (85–125 nm) solar irradiance during event (red) and quiet-time (blue). (c) Integrated SXR (magenta) and EUV (black) variations with event/quiet-time marked by dotted lines. (d) Solar wind electron flux and (e) SEP 1-f total electron/ion energy fluxes versus altitude for event (red) and quiet-time (blue).

Magnetometer, and SWEA instruments onboard the MAVEN spacecraft. The results obtained after analyzing the muti-spacecraft data sets are described in the following paragraphs.

Figure 1 represents Enlil-Cone model inner heliospheric simulation snapshot of the ICME (left) and, on the right, temporal variation of the upstream solar wind (a) density, (b) velocity, (c) dynamic pressure (SWDP), (d) IMF (|**B**|), and (e) electron flux, respectively, between 08 and 17 May 2019. Similarly, Figures S1 and S5 in Supporting Information S1 show the Enlil-Cone model snapshots and upstream solar wind parameter variations for the ICME events on 24 July and 21 August 2022. For obtaining the unhindered solar wind intervals in the upstream region, we have followed the algorithm provided by Halekas et al. (2017) and Ram et al. (2023). The solar wind parameters (density, velocity, and dynamic pressure), and resultant IMF (|**B**|) show an upsurge on 09 May 2019, and attain peak magnitudes of ~12 cm^{-3}, 320 km s^{-1}, and 1.6 nPa, respectively, on 10 May 2019. During this period, the peak magnitude of IMF (|**B**|) and electron flux approach to 17.5 nT and 10^8 eV cm^{-2}s^{-1}sr^{-1}, respectively. This ICME event shares similar strength with the 14 June 2007 ICME event reported by Ritter et al. (2018). Both events exhibit comparable enhancements in solar wind velocity, forming the basis for their comparison. The vertical-colored dotted line in red represents the NOMAD-UVIS observation during the event-time (11 May 2019 00:20 UT), whereas the blue-colored dotted line depicts the quiet-time (15 May 2019 15:38 UT) condition. Although, the event-time observation (NOMAD-UVIS limb observation) does not coincide with the peak time of ICME, it occurred during the declining phase of the ICME.

Figure 2 shows the EUVM observations during the respective days of May 2019. The panels (a) and (b) in Figure 2 represent the solar irradiance flux for soft X-ray (SXR; 1–10 nm) and EUV (85–125 nm). The red and blue curves denote the solar irradiance flux during the event and quiet-times, respectively. Figure 2c depicts the variation of integrated SXR and EUV flux between 08 and 17 May 2019. We have calculated the integrated SXR

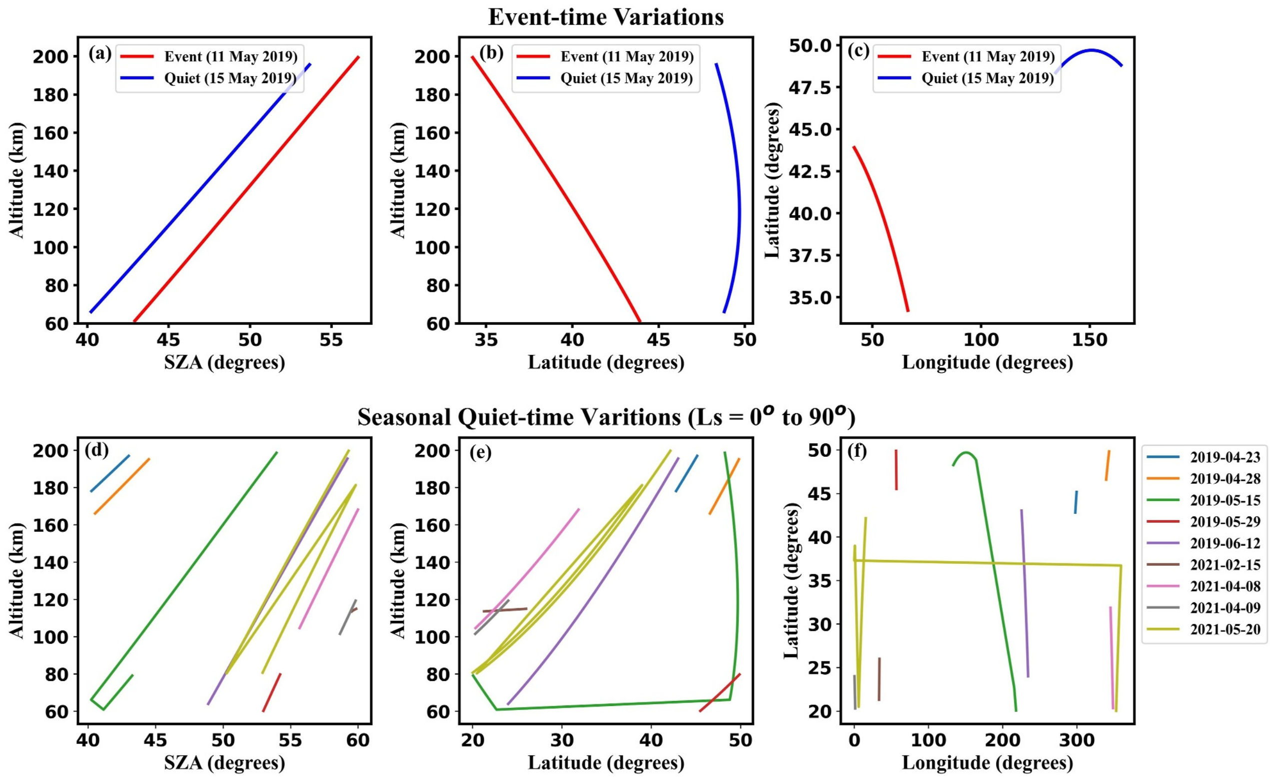

Figure 3. Variation of (a) solar zenith angle, (b) latitude with altitude and (c) longitude during the event- (red) and quiet-time (blue). Seasonal quiet-time variations are shown in (d), (e), and (f).

(right *y*-axis) and EUV (left *y*-axis) from Figures 2a and 2b. The red- and blue-colored dotted lines represent the UVIS observations for the event and quiet-times (like Figure 1). Figures 2d and 2e show the variation of solar wind electron energy (100–500 eV) flux and SEP 1-f total electron/ion energy fluxes with altitude for event (red) and quiet-time (blue). During the event-time, the SXR flux reaches approximately 5×10^{-6} $W\text{m}^{-2}\text{nm}^{-1}$, while during the quiet-time, it is about 4.6×10^{-6} $W\text{m}^{-2}\text{nm}^{-1}$. This represents ~8% increase in the soft X-ray flux compared to the quiet-time. The SXR flux during ICMEs of 24 July and 21 August 2022 shows an enhancement compared to their respective seasonal-average quiet-time flux [Figures S2a and S6a in Supporting Information S1]. The EUV flux during the event-time does not show any significant change as compared to that of quiet-time, evident from Figures 2b and 2c. Similar behavior is observed during 24 July and 21 August 2022 events [Figures S2b and S6b in Supporting Information S1]. Moreover, below 200 km, the solar wind electron energy flux and SEP total electron (ion) energy flux increased by ~4.2 and ~8.2 (~13.42) times respectively during the event-time compared to quiet-time (Figures 2d and 2e). Similarly, during the events on 24 July and 21 August 2022, these fluxes got enhanced by ~2.19 and ~4.74 (~3.07) and ~2.43 and ~5.72 (~5.16) times respectively compared to their seasonal-averaged quiet-time near 200 km [Figures S2c–e, S6c–e in Supporting Information S1].

Figures 3a and 3b illustrate the variation of SZA and latitude with respect to altitude for the event (red line; Ls: ~23.4) and quiet-time (blue line; Ls: ~25.6) limb observations using NOMAD-UVIS. For obtaining a similar SZA and latitude coverage of the event and quiet-time limb profiles, the egress and ingress limb scans have been considered, respectively. In the altitude range of 60–200 km, the event-time limb profile covers the SZA and latitude range of 43.3°–56.6° and 43.7°–34.2°, respectively. Whereas, the quiet-time limb profile falls within the SZA and latitude range of 40.6°–53.5° and 48.9°–48.4° respectively. In addition, Figure 3c shows the spatial distribution of limb observations in latitude and longitude. Similarly, Figures 3d and 3e depict the variation of SZA and latitude with altitude for the Seasonal Quiet-time profiles whereas, Figure 3f shows its spatial variation. The SZA and spatial variation of 24 July and 21 August 2022 events and their seasonal-averaged quiet-time profiles are shown in Figures S3 and S7 in Supporting Information S1, respectively.

10.1029/2024GL111745

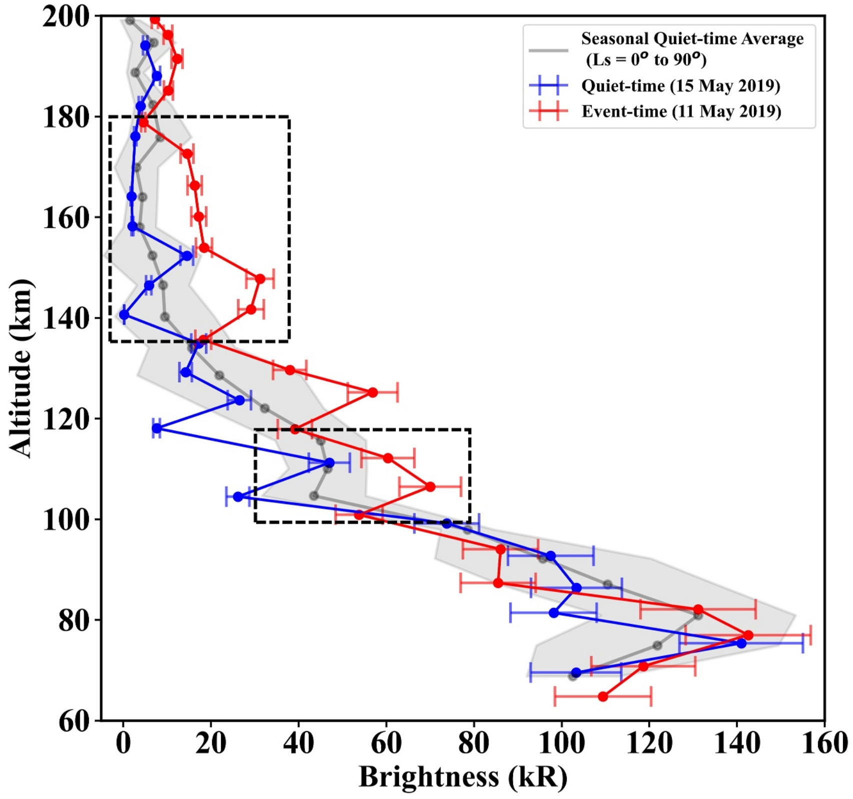

Figure 4. Radiance limb profile of 557.7 nm emission during event-time (red), quiet-time (blue), and average-quiet-time (gray). Gray zone is 1σ variability. Red and blue horizontal bars are 10% error in the brightness.

Since NOMAD-UVIS dayside inertial limb observations occur intermittently, it is difficult to obtain consecutive observations. This major constraint has made it challenging to find UVIS observation during ICME events along with the quiet-time observation having similar SZA and location. Thus, we could only find the ICME event of 09–11 May 2019 with a nearby quiet-time observation of 15 May 2019 satisfying the criteria necessary for this study. Figure 4 depicts the variation of the 557.7 nm emission as a function of altitude. The x-axis represents brightness (kR), and the y-axis denotes the tangent altitude (60–200 km). The red, blue, and gray-colored profiles show the event-time, quiet-time, and seasonal quiet-time average NOMAD-UVIS limb observations. The event and quiet-time profiles are generated by averaging the brightness values in 6 km altitude bin. The profiles (red and blue) are represented with their respective measurement uncertainties in horizontal error bars. To provide a typical background scenario during the northern spring season (Ls: 0°–90°; Latitude: 20°–60°), we have considered the UVIS inertial limb mode observations, including both the egress and ingress scans. We have considered those profiles which are distributed over different longitudes to ensure that the profiles lie within the similar latitude and SZA ranges (mentioned in Figure 3) on 11 and 15 May 2019. Additionally, quiet-time profiles with SZA nearly within ±5° of the event-time profile at all altitudes, have been considered. After applying these constraints, 9 quiet-time profiles have been obtained. The seasonal quiet-time average limb profile (gray) is calculated by taking the mean of all the quiet-time profiles in 6 km attitude bins. The gray profile is shown with the 1σ variability (gray-zone). The purpose of calculating the seasonal quiet-time average of 557.7 nm limb profile is to assess typical background brightness at different altitudes during quiet-time conditions. The primary emission peak magnitude of brightness during event-time (red) does not show a significant deviation in comparison to the quiet-time (blue). Also, the primary emission peak brightness lies within the 1σ uncertainty of seasonal quiet-time average (gray-zone), showing that the brightness of primary emission peak of some quiet-time observations is greater than that of event-time. This could be related to the variation of 557.7 nm emission with latitude, longitude or SZA (Soret et al., 2022). During the event, the primary emission peak brightness is 142.5 ± 14.2 kR at 77 km altitude. Whereas, for the quiet-time, the magnitude is 141 ± 14 kR (75 km altitude). The seasonal quiet-time average brightness for the primary emission peak is 127 ± 43.7 kR at an altitude of 81 km.

It is interesting to note that the 557.7 nm emission brightness on the event-time show an enhancement at the secondary emission peak (70 ± 7 kR; 106.5 km altitude) compared to the both quiet-time (47 ± 4.7 kR; 111.2 km altitude) and seasonal quiet-time average (47 ± 11.8 kR; 111.4 km altitude) profiles. Further, there is a noticeable increase in the brightness of event-time between 140 and 180 km altitude. The enhancement in brightness is more than quiet-time profile and lies beyond the 1σ variability of seasonal quiet-time average. The increase in brightness of secondary emission peak and upper altitude region is also observed in the 24 July and 21 August 2022 profiles compared to their respective 1σ uncertainty of seasonal quiet-time profiles (Figures S4 and S8 in Supporting Information S1). For verifying this observed enhancement in the brightness, we applied the statistical *t*-test (Mann-Whitney *U* test; Mann & Whitney, 1947) on the data set [available in Sharma et al. (2024)] between the altitude of 100–180 km. The *t*-test determines if there is a significant brightness difference between event-time and quiet-time, assuming no significant difference under the null hypothesis (p-value > 0.05). The *t*-test results show p-values of ~0.0013 between event-time and quiet-time, ~0.029 between event-time and seasonal quiet-time average, and ~0.182 between quiet-time and seasonal quiet-time average. For the 24 July and 21 August 2022 events, the p-values are ~0.0012 and ~0.0166, respectively. p-values under 0.05 indicate a significant difference, confirming that event-time data differs significantly from both quiet-time and seasonal quiet-time averages.

4. Discussion and Conclusion

The present case study deals with the impact of the ICME (10–11 May 2019) on the Martian $O(^1S)$ 557.7 nm dayglow emission using the NOMAD-UVIS observations onboard ExoMars-TGO orbiter. Past and current space missions to Mars have detected various atomic oxygen emissions in UV (Barth et al., 1971), however, visible emissions have been discovered quite recently (Gérard et al., 2020, 2021; Soret et al., 2022). The $O(^1S)$ 557.7 nm is one of the visible emissions produced by the forbidden transition from the $O(^1S)$ to the O (^1D) state of atomic oxygen (Fox & Dalgarno, 1979).

Previous theoretical works investigated the photochemistry of the $O(^1S)$ state of atomic oxygen and predicted the radiance limb profile of $O(^1S)$ 557.7 nm emission in the Martian atmosphere (Fox & Dalgarno, 1979; Gérard et al., 2020; Gkouvelis et al., 2018; Raghuram et al., 2021). The radiance limb profiles of the 557.7 nm emission are in good agreement with the models having the primary and secondary emission peaks between the altitude range of 75–80 km and 110–120 km, respectively. These studies have shown that reactions R1–R9 are primarily responsible for producing the $O(^1S)$ state. The photodissociation of CO_2 by solar H Lyman-α (121.6 nm) radiation is the dominant factor in producing the $O(^1S)$ state and forming the primary emission peak of the 557.7 nm emission. The secondary emission peak is mainly formed by photodissociation of CO_2 through EUV (86–116 nm) radiation (Gérard et al., 2020; Raghuram et al., 2021). Other processes, such as dissociative recombination of O_2^+ (R7) electron impact on O, CO, and CO_2, also contribute to the formation of the secondary emission peak, with dissociative recombination of O_2^+ being the second most crucial process in secondary emission peak formation (Gkouvelis et al., 2018).

In the present case studies, we assess the impact of the ICME on the Martian 557.7 nm dayglow emission. The observations from the SWIA, MAG, and SWEA instruments onboard the MAVEN spacecraft indicate a significant increase in the magnitude of solar wind parameters, IMF (|**B**|) and electron flux during the passage of an ICME event during 09–11 May 2019 compared to quiet-time. Using the observations from the NOMAD-UVIS onboard the ExoMars-TGO during both event-time (11 May 2019) and quiet-time (15 May 2019), we investigate the impact of ICME on the Martian 557.7 nm dayglow emission at different altitudes. It is evident from Figure 4 that the magnitude of the primary emission peak during the event-time does not show significant variation in comparison to the quiet-time and lies within the 1σ uncertainty of seasonal quiet-time average profile. This lack of variation in the brightness of primary emission peak during the event-time might be due to photodissociation of CO_2 by solar H Lyman-α. As illustrated in Figure 2b, the solar H Lyman-α flux exhibits little difference between event and quiet-time, which explains the negligible change observed in the brightness of primary emission peak in the event-time profile.

During the event, the secondary emission peak brightness increased significantly (~49%) along with upper altitude region compared to quiet-time. Since the EUV flux between 86 and 115 nm is approximately similar for both event and quiet-times (Figures 2b and 2c), the enhancement in the brightness during event-time might be attributed to electron impact processes R4–R9. During the ICME event, the electron flux (5–100 eV) increased nearly twice that of quiet-time period (Figure 1e), and the X-ray flux also increased by ~8%. These photo-electrons having enough kinetic energy to produce secondary electrons (Jain, 2013). Additionally, the SEP total electron (ion) energy flux and solar wind electron flux (100–500 eV) increased ~8.85 (~13.42) times and ~4.2 times below 200 km altitude respectively during event-time (Figure 3). Similar enhancements are also observed during 24 July and 21 August 2022 events (Figures S2 and S6 in Supporting Information S1). This large increase in the electron/ion fluxes can enhance the ionization that can further produce secondary electrons below 300 km altitude (Felici et al., 2024; Nakamura et al., 2022). Furthermore, during the ICME, high-energy solar wind electrons can also directly impact the CO_2 molecules. Therefore, the combined impact of photo-electrons, ionization induced by high-energy solar-wind particles and their direct impact on CO_2 might have caused enhancement in electron impact processes R4–R9, resulting in increased brightness at secondary emission peak and upper altitude of 557.7 nm emission. Additionally, we observed enhancement in the brightness of 297.2 nm dayglow (measured using MAVEN-IUVS (Imaging Ultraviolet Spectrograph)) during ICME over a wide range of altitude (Figures S9 and S10 in Supporting Information S1). However, detailed analysis is beyond the scope of this work. This specific case study, for the first time, provides us an opportunity wherein we assess the impact of an ICME on the Martian atmospheric 557.7 nm dayglow emission.

We have investigated the impact of this ICME event, which is categorized as minor storm (NASA DONKI archive), on 557.7 nm emission. However, future studies could explore whether stronger ICMEs amplify the secondary emission peak and upper altitude brightness more significantly. This present work paves the way to carry out more research in the future with more comprehensive data sets. Since these findings are only based on a few ICME events, further analyses with more ICME events will be required in the future to firmly establish our current conclusions.

To summarize, this study reports the impact of an ICME event (11 May 2019) on the Martian 557.7 nm dayglow emission using MAVEN and NOMAD-UVIS data sets. During this event, the primary emission peak brightness showed similar behavior as quiet-time (15 May 2019). This behavior of the primary emission peak is attributed to the minimal change in the solar H Lyman-α flux in the period of ICME. On the contrary, the brightness of the secondary emission peak and higher altitude region (140–180 km) showed noticeable increase during the ICME as compared to quiet-time. Interestingly, this enhancement in brightness aligns with the increase in solar wind electron flux, SEP electron/ion fluxes and SXR flux, secondary electrons and thereby increased the electron impact processes. Additionally, the direct impact of energetic electrons on CO_2 likely contributed to the brightness enhancement. Hence, during ICMEs, the combined effects of photoelectrons, ionization induced by high-energy solar wind particles, and their direct interaction with CO_2 contributed to the enhancement of both the secondary emission peak brightness and the upper altitude region compared to quiet-time conditions. This case study shows that external forcing like ICME enhances the brightness of the secondary emission peak and upper altitude region.

Data Availability Statement

We have used the NASA DONKI catalog for space weather forecast information. MAVEN data set of SWIA (solar-wind ion) Level 2, version_19, revision_01, MAG (IMF) Level 2, version_19, revision_01, SWEA (electron-flux) Level 2, version_19, revision_01, and EUV Monitor Level 3, version_15, revision_01 used in this work are obtained from the NASA Planetary Data System (PDS) at PDS/PPI Home Page (https://pds-ppi.igpp.ucla.edu/search/default.jsp). NOMAD-UVIS Level 3 Calibrated data can be downloaded from ESA Planetary Science Archive (PSA) at PSA UI (https://archives.esac.esa.int/psa/#!Table%20View). NOMAD-UVIS datafiles that is, nmd_cal_sc_uvis_20190510t233028-20190511t004353-l and nmd_cal_sc_uvis_20190515t153813-20190515t165133-l have been utilized for the event and quiet-time observation, respectively. NOMAD-UVIS derived data products used in this work can be found in Sharma et al. (2024).

Acknowledgments
We sincerely acknowledge the ESA PSA and ExoMars-TGO NOMAD-UVIS team for the spectral data. We also acknowledge the NASA PDS and MAVEN team members, especially SWIA and SWEA for the data sets. A.R.S., D.P., and L.R. acknowledge the fellowship from the Ministry of Education, Government of India for carrying out this research work. L.S. and J.C.G. acknowledge funding for this research by the PRODEX program of the European Space Agency, managed in collaboration with the Belgian Federal Science Policy Office. This work is also supported by the Ministry of Education, Government of India.

References

Andersson, L., Ergun, R. E., Delory, G. T., Eriksson, A., Westfall, J., Reed, H., et al. (2015). The Langmuir Probe and Waves (LPW) instrument for MAVEN. *Space Science Reviews*, *195*(1–4), 173–198. https://doi.org/10.1007/s11214-015-0194-3

Aoki, S., Gkouvelis, L., Gérard, J.-C., Soret, L., Hubert, B., Lopez-Valverde, M. A., et al. (2022). Density and temperature of the upper mesosphere and lower thermosphere of Mars retrieved from the OI 557.7 nm dayglow measured by TGO/NOMAD. *Journal of Geophysical Research: Planets*, *127*(6), e2022JE007206. https://doi.org/10.1029/2022JE007206

Barth, C. A., Hord, C. W., Pearce, J. B., Kelly, K. K., Anderson, G. P., & Stewart, A. I. (1971). Mariner 6 and 7 ultraviolet spectrometer experiment: Upper atmosphere data. *Journal of Geophysical Research*, *76*(10), 2213–2227. https://doi.org/10.1029/JA076i010p02213

Bougher, S. W., Roeten, K. J., Olsen, K., Mahaffy, P. R., Benna, M., Elrod, M., et al. (2017). The structure and variability of Mars dayside thermosphere from MAVEN NGIMS and IUVS measurements: Seasonal and solar activity trends in scale heights and temperatures. *Journal of Geophysical Research: Space Physics*, *122*(1), 1296–1313. https://doi.org/10.1002/2016JA023454

Connerney, J. E. P., Espley, J., Lawton, P., Murphy, S., Odom, J., Oliversen, R., & Sheppard, D. (2015). The MAVEN magnetic field investigation. *Space Science Reviews*, *195*(1–4), 257–291. https://doi.org/10.1007/s11214-015-0169-4

Connerney, J. E. P., Espley, J. R., DiBraccio, G. A., Gruesbeck, J. R., Oliversen, R. J., Mitchell, D. L., et al. (2015). First results of the MAVEN magnetic field investigation. *Geophysical Research Letters*, *42*(21), 8819–8827. https://doi.org/10.1002/2015GL065366

Eparvier, F. G., Chamberlin, P. C., Woods, T. N., & Thiemann, E. M. B. (2015). The solar extreme ultraviolet monitor for MAVEN. *Space Science Reviews*, *195*(1–4), 293–301. https://doi.org/10.1007/s11214-015-0195-2

Fallows, K., Withers, P., & Gonzalez, G. (2015). Response of the Mars ionosphere to solar flares: Analysis of MGS radio occultation data. *Journal of Geophysical Research: Space Physics*, *120*(11), 9805–9825. https://doi.org/10.1002/2015JA021108

Felici, M., Segale, J., Withers, P., Lee, C. O., Hughes, A., Thiemann, E., et al. (2024). Impacting the dayside Martian ionosphere from above and below: Effects of the impact of CIRs and ICMEs close to aphelion (April 2021) and during dust storms (June/July 2022) seen with MAVEN ROSE. *Icarus*, *424*, 116089. https://doi.org/10.1016/j.icarus.2024.116089

Fox, J. L. (2004). Response of the Martian thermosphere/ionosphere to enhanced fluxes of solar soft X rays. *Journal of Geophysical Research*, *109*(A11), A11310. https://doi.org/10.1029/2004JA010380

Fox, J. L., & Dalgarno, A. (1979). Ionization, luminosity, and heating of the upper atmosphere of Mars. *Journal of Geophysical Research*, *84*(A12), 7315–7333. https://doi.org/10.1029/JA084iA12p07315

Fox, J. L., & Yeager, K. E. (2006). Morphology of the near-terminator martian ionosphere: A comparison of models and data. *Journal of Geophysical Research*, *111*(A10), A10309. https://doi.org/10.1029/2006JA011697

Gérard, J. C., Aoki, S., Gkouvelis, L., Soret, L., Willame, Y., Thomas, I. R., et al. (2021). First observation of the oxygen 630 nm emission in the martian dayglow. *Geophysical Research Letters*, *48*(8), e2020GL092334. https://doi.org/10.1029/2020GL092334

Gérard, J. C., Aoki, S., Willame, Y., Gkouvelis, L., Depiesse, C., Thomas, I. R., et al. (2020). Detection of green line emission in the dayside atmosphere of Mars from NOMAD-TGO observations. *Nature Astronomy*, *4*(11), 1049–1052. https://doi.org/10.1038/s41550-020-1123-2

Gkouvelis, L., Gérard, J. C., Ritter, B., Hubert, B., Schneider, N. M., & Jain, S. K. (2018). The O(1S) 297.2-nm dayglow emission: A tracer of CO_2 density variations in the martian lower thermosphere. *Journal of Geophysical Research: Planets*, *123*(12), 3119–3132. https://doi.org/10.1029/2018JE005709

Halekas, J. S., Ruhunusiri, S., Harada, Y., Collinson, G., Mitchell, D. L., Mazelle, C., et al. (2017). Structure, dynamics, and seasonal variability of the Mars-solar wind interaction: MAVEN solar wind ion analyzer in-flight performance and science results. *Journal of Geophysical Research: Space Physics*, *122*(1), 547–578. https://doi.org/10.1002/2016JA023167

Halekas, J. S., Taylor, E. R., Dalton, G., Johnson, G., Curtis, D. W., McFadden, J. P., et al. (2015). The solar wind ion analyzer for MAVEN. *Space Science Reviews*, *195*(1–4), 125–151. https://doi.org/10.1007/s11214-013-0029-z

Jain, S. K. (2013). *Dayglow Emissions on Mars and Venus (Ph.D. Thesis)*. Cochin University of Science and Technology. Retrieved from http://dyuthi.cusat.ac.in/purl/3688

Jakosky, B. M., Grebowsky, J. M., Luhmann, J. G., Connerney, J., Eparvier, F., Ergun, R., et al. (2015). MAVEN observations of the response of Mars to an interplanetary coronal mass ejection. *Science*, *350*, 6261. https://doi.org/10.1126/science.aad0210

Jakosky, B. M., Lin, R. P., Grebowsky, J. M., Luhmann, J. G., Mitchell, D. F., Beutelschies, G., et al. (2015). The Mars atmosphere and volatile evolution (MAVEN) mission. *Space Science Reviews*, *195*(1–4), 3–48. https://doi.org/10.1007/s11214-015-0139-x

Larson, D. E., Lillis, R. J., Lee, C. O., Dunn, P. A., Hatch, K., Robinson, M., et al. (2015). The MAVEN solar energetic particle investigation. *Space Science Reviews*, *195*(1–4), 153–172. https://doi.org/10.1007/s11214-015-0218-z

López-Valverde, M. A., Gérard, J. C., González-Galindo, F., Vandaele, A. C., Thomas, I., Korablev, O., et al. (2018). Investigations of the Mars upper atmosphere with ExoMars trace gas orbiter. *Space Science Reviews*, *214*(1), 29. https://doi.org/10.1007/s11214-017-0463-4

Mann, H. B., & Whitney, D. R. (1947). On a test of whether one of two random variables is stochastically larger than the other, the annals of mathematical statistics. *The Annals of Mathematical Statistics*, *18*(1), 50–60. https://doi.org/10.1214/aoms/1177730491

Mendillo, M., Withers, P., Hinson, D., Rishbeth, H., & Reinisch, B. (2006). Effects of solar flares on the ionosphere of Mars. *Science*, *311*(5764), 1135–1138. https://doi.org/10.1126/science.1122099

Mitchell, D. L., Mazelle, C., Sauvaud, J. A., Thocaven, J. J., Rouzaud, J., Fedorov, A., et al. (2016). The MAVEN solar wind electron analyzer. *Space Science Reviews*, *200*(1–4), 495–528. https://doi.org/10.1007/s11214-015-0232-1

Nakamura, Y., Terada, N., Leblanc, F., Rahmati, A., Nakagawa, H., Sakai, S., et al. (2022). Modeling of diffuse auroral emission at Mars: Contribution of MeV protons. *Journal of Geophysical Research: Space Physics*, *127*(1), e2021JA029914. https://doi.org/10.1029/2021JA029914

Patel, M. R., Antoine, P., Mason, J., Leese, M., Hathi, B., Stevens, A. H., et al. (2017). NOMAD spectrometer on the ExoMars trace gas orbiter mission: Part 2—Design, manufacturing, and testing of the ultraviolet and visible channel. *Applied Optics*, *56*(10), 2771–2782. https://doi.org/10.1364/AO.56.002771

Raghuram, S., Jain, S. K., & Bhardwaj, A. (2021). Forbidden atomic oxygen emissions in the martian dayside upper atmosphere. *Icarus*, *359*, 114330. https://doi.org/10.1016/j.icarus.2021.114330

Ram, L., Rout, D., Rathi, R., Mondal, S., Sarkhel, S., & Halekas, J. (2023). A comparison of the impacts of CMEs and CIRs on the martian dayside and nightside ionospheric species. *Journal of Geophysical Research: Planets*, *128*(4), e2022JE007649. https://doi.org/10.1029/2022JE007649

Ram, L., Rout, D., Rathi, R., Withers, P., & Sarkhel, S. (2024). Martian M2 peak behavior in the dayside near-terminator ionosphere during interplanetary coronal mass ejections. *Icarus*, *408*, 115857. https://doi.org/10.1016/j.icarus.2023.115857

Ram, L., Sharma, R., Rout, D., Rathi, R., & Sarkhel, S. (2024). Investigation on the impact of solar flares on the Martian atmospheric emissions in the dayside near-terminator region: Case studies. *Journal of Geophysical Research: Planets*, *129*(8), e2024JE008315. https://doi.org/10.1029/2024JE008315

Rishbeth, H., & Mendillo, M. (2004). Ionospheric layers of Mars and earth. *Planetary and Space Science*, *52*(9), 849–852. https://doi.org/10.1016/j.pss.2004.02.007

Ritter, B., Gérard, J. C., Hubert, B., Rodriguez, L., & Montmessin, F. (2018). Observations of the proton aurora on Mars with SPICAM on board Mars express. *Geophysical Research Letters*, *45*(2), 612–619. https://doi.org/10.1002/2017GL076235

Sharma, A. R., Sarkhel, S., Suhaag, H., Ram, L., Patgiri, D., Soret, L., et al. (2024). A case study on the impact of interplanetary coronal mass ejection on the Martian O(1S) 557.7 nm dayglow emission using ExoMars TGO/NOMAD-UVIS observations: First Results [Dataset]. *Zenodo*. https://doi.org/10.5281/zenodo.12690459

Soret, L., Gérard, J. C., Aoki, S., Gkouvelis, L., Thomas, I. R., Ristic, B., et al. (2022). The Mars oxygen visible dayglow: A martian year of NOMAD/UVIS observations. *Journal of Geophysical Research: Planets*, *127*(6), e2022JE007220. https://doi.org/10.1029/2022JE007220

Space Weather Database of Notifications. (2010). Knowledge, and information (DONKI) [Software]. In *Donki*. Retrieved from https://kauai.ccmc.gsfc.nasa.gov/DONKI/search/

Thampi, S. V., Krishnaprasad, C., Nampoothiri, G. G., & Pant, T. K. (2021). The impact of a stealth CME on the Martian topside ionosphere. *Monthly Notices of the Royal Astronomical Society*, *503*(1), 625–632. https://doi.org/10.1093/mnras/stab494

Vandaele, A., Willame, Y., Depiesse, C., Thomas, I., Robert, S., Bolsée, D., et al. (2015). Nomad team, optical and radiometric models of the NOMAD instrument part I: The UVIS channel. *Optics Express*, *23*, 30028–30042. https://doi.org/10.1364/OE.23.030028

Vandaele, A. C., Lopez-Moreno, J. J., Patel, M. R., Bellucci, G., Daerden, F., Ristic, B., et al. (2018). NOMAD, an integrated suite of three spectrometers for the ExoMars trace gas mission: Technical description, science objectives and expected performance. *Space Science Reviews*, *214*(5), 80. https://doi.org/10.1007/s11214-018-0517-2

Withers, P. (2020). Are sporadic plasma layers at 90 km in the Mars ionosphere produced by solar energetic particle events. *Journal of Geophysical Research: Space Physics*, *125*(9), e2020JA028120. https://doi.org/10.1029/2020JA028120

Withers, P., Felici, M., Mendillo, M., Moore, L., Narvaez, C., Vogt, M. F., & Jakosky, B. M. (2018). First ionospheric results from the MAVEN radio occultation science experiment (ROSE). *Journal of Geophysical Research: Space Physics*, *123*(5), 4171–4180. https://doi.org/10.1029/2018JA025182